

# Singular integration towards a spectrally accurate finite difference operator

By ANDRÉ NACHBIN\*

## Abstract

It is an established fact that a finite difference operator approximates a derivative with a fixed algebraic rate of convergence. Nevertheless, we exhibit a new finite difference operator and prove it has spectral accuracy. Its rate of convergence is not fixed and improves with the function's regularity. For example, the rate of convergence is exponential for analytic functions. Our new framework is conceptually nonstandard, making no use of polynomial interpolation, nor any other expansion basis, such as typically considered in approximation theory. Our new method arises solely from the numerical manipulation of singular integrals, through an accurate quadrature for Cauchy Principal Value convolutions. The kernel is a distribution which gives rise to multi-resolution grid coefficients. The respective distributional finite difference scheme is spatially structured having stencils of different support widths. These multi-resolution stencils test/estimate function variations in a nonlocal fashion, giving rise to a highly accurate distributional finite difference operator. Computational illustrations are presented, where the accuracy and roundoff error structure are compared with the respective Fourier based method. We also compare our method with a recent and popular complex-step method.

## 1 Introduction and background

Finite difference operators (FDO) are an important tool for solving differential equations in an approximate form. Finite difference methods (FDM)

---

\*Address for correspondence: André Nachbin, IMPA, Estrada Dona Castorina 110, Jardim Botânico, Rio de Janeiro, RJ, Brazil, CEP 22460-320; e-mail: nachbin@impa.br

are used in computations as well as in proofs where, for example, a semi-discretization can lead to an existence proof. Finite difference approximations typically arise from polynomial interpolation or truncating Taylor expansions. In the present work a completely different framework is adopted.

In their classical book [6], Richtmyer and Morton consider an example with the heat equation  $u_t = \sigma u_{xx}$  and provide the convergence rate for the following FDM:

$$\frac{u_j^{n+1} - u_j^n}{\Delta t} = \sigma \frac{u_{j+1}^n - 2u_j^n + u_{j-1}^n}{\Delta x^2}, \quad j = 1, 2, \dots, J-1; \quad n = 0, 1, \dots,$$

with initial condition

$$u_j^0 = \varphi(j\Delta x), \quad j = 1, 2, \dots, J-1,$$

and boundary conditions  $u_0^n = u_J^n = 0$ ,  $n = 0, 1, \dots$ . The interval  $[0, L = J\Delta x]$  is partitioned by a uniform grid in space. At a discrete time  $t^n = n\Delta t$  the FDM solution at node  $x_j = j\Delta x$  is denoted by  $u_j^n$ , whereas  $u = u(x_j, t^n)$  is the heat equation solution evaluated on the grid. For an initial heat profile  $\varphi(x) \in C^p$  the following convergence rates, in space and time, are obtained ([6], page 23):

$$u_j^n - u = \begin{cases} \mathcal{O}(\Delta t^{p/4}) = \mathcal{O}(\Delta x^{p/2}), & \text{for } p \leq 3, \\ \mathcal{O}(\Delta t |\log \Delta t|) = \mathcal{O}(\Delta x^2 |\log \Delta x|), & \text{for } p = 4, \\ \mathcal{O}(\Delta t) = \mathcal{O}(\Delta x^2), & \text{for } p > 4. \end{cases} \quad (1)$$

Relevant to the present work, one observes a convergence rate partially depending on the regularity of the initial data. For a piecewise-linear initial temperature distribution, the FDM's error decreases as a square root with respect to the mesh-size. On the other extreme, for an analytic function  $\varphi(x)$  the error does not decay any faster than  $\mathcal{O}(\Delta x^2)$ . The centered difference operator in space, is of second order. Irrespective of the importance of FDMs, Richtmyer and Morton [6] mention that *"In any case, however, finite-difference methods for partial differential equations seldom achieve more than a modest accuracy"*. Fornberg [4], among others, investigated higher order difference operators for approximating a first derivative. For a fixed number of grid points  $N$ , Fornberg deduced optimal coefficients in the operator representation. Fornberg in Table 1 [4] displays the coefficients for operators using up to 60 grid points and having an order of accuracy  $\mathcal{O}(\Delta x^p)$ , with  $p = 120$ .

In the present work we prove an unexpected result providing the existence of a finite difference operator with spectral accuracy. Namely a discrete operator where the truncation error improves with the regularity of the underlying function. As will be shown, our new discrete operator is based

on singular integration which generates a family of second order difference operators, as above. Spectral accuracy is then achieved through (multi-resolution) combinations of these lower order approximations. A striking point is that multi-resolution arises from the fact that the kernel of the integral operator is a distribution. We do not use a polynomial approximation as in FDMs, nor invoke a trigonometric basis as in spectral methods. Our spectrally accurate FDO arises naturally from the numerical manipulation of singular integrals, namely Hilbert transforms. Harmonic conjugation plays an interesting role as will be discussed together with the popular (complex-step) method introduced by Squire and Trapp [8] and recently advertised by Higham [5]. The complex-step method aims at reducing the truncation error by successfully allowing extremely small step sizes. In contrast, in our method the truncation error will be (conceptually) small in the case of smooth functions. Very small step sizes are not needed. The key to this fact is the spectrally accurate quadrature of singular integrals.

## 2 Singular integrals and quadrature

Sidi and Israeli [7] proved the spectral accuracy of a numerical quadrature for periodic singular integrals, defined in the Cauchy Principal Value sense. Spectral accuracy is a remarkable property for a numerical method, where the error depends on the smoothness of the function. If the function is analytic the error decays exponentially. If the function is band-limited, the quadrature is exact up to roundoff error. Hence it is also known as exponential convergence or infinite-order accuracy [3]. Spectral-accuracy properties are precisely defined in Fourier space by combining the Paley-Wiener theorem with the Poisson summation formula [9].

From the work of Sidi and Israeli, theorems 7(a) and 8 play a role in our theorem and therefore are respectively reproduced below, in a convenient notation.

**Theorem 1.** *Consider the singular integral  $I = \int_a^b G(x)dx$ , where the  $L$ -periodic integrand has a pole at  $x = y$ , thus being represented in the form  $G(x) = g(x)/(x - y) + \tilde{g}(x)$ . Assume that the functions  $g(x)$  and  $\tilde{g}(x)$  are  $2m$  times differentiable on  $[a, b]$ . Let the grid spacing be  $h = L/N$ . Letting  $y = x_k$ , the quadrature given by*

$$Q_N[G] \equiv h \sum_{\substack{j=1 \\ j \neq k}}^N G(x_j)$$

yields the error

$$E_N[G] = I - Q_N[G] = (g(y) + \tilde{g}(y))h + \mathcal{O}(h^{2m}), \quad \text{as } h \rightarrow 0.$$

This quadrature skips the singular point and the error is of first order in  $h$ . Nevertheless, the next order error-term depends on the regularity of the functions  $g$  and  $\tilde{g}$ . Sidi and Israeli [7] then used a Richardson extrapolation to take advantage of this fact, namely canceling the lower order term and thus obtaining spectral accuracy on the coarser grid. This follows from

**Theorem 2.** Consider  $G(x)$  and the quadrature  $Q_N[G]$  as in Theorem 1, with  $h = h_N \equiv L/N$ . Perform the Richardson extrapolation

$$\tilde{Q}_N[G] = 2Q_{2N}[G] - Q_N[G] = h_N \sum_{j=1}^N G(a + jh_N - 0.5h_N).$$

$\tilde{Q}_N[G]$  is a midpoint rule approximation and

$$\tilde{E}_N[G] = I - \tilde{Q}_N[G] = \mathcal{O}(h^{2m}), \quad \text{as } h_N \rightarrow 0.$$

$\tilde{Q}_N[G]$  is also known as the alternate trapezoidal rule (ATR) as depicted in figure 1. If the integrand's singularity is, for example, at the node indicated by a circle, then the singular integral is calculated on what we will call the *adjoint grid*, indicated by the squares. This leads to spectral accuracy on a grid of spacing  $2h$ .

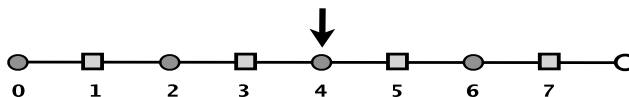


Figure 1: Grid for the alternate trapezoidal rule (ATR). Two alternating grids: one with square nodes and the other with circular nodes. For example in the case of a convolution with a distribution, if the kernel blows up at node 4 as indicated by the arrow, only the adjoint grid with square nodes is used. The last white node calls attention to an existing periodic condition, namely  $0 \equiv 8$ .

## 2.1 The distributional finite difference method

We define several grid levels labelled by  $\ell$ , having in mind multi-resolution. In our study only odd-levels  $\ell = 1, 3, \dots$  will arise. On a resolution level- $\ell$  the

grid spacing is  $\ell h$  and the standard second order (centered) finite difference operator is given by

$$D_{j,\ell}^2[f] \equiv \frac{f_{j-\ell} - 2f_j + f_{j+\ell}}{(\ell h)^2}. \quad (2)$$

This discrete operator approximates the second derivative  $f''(x)$  at the mesh point  $x = x_j$ . It will become clear why this approximation to a second derivative is relevant in the present study. Associated with this discrete operator we have a 3-point stencil, supported over  $2\ell + 1$  nodes indicating its resolution.

As in the previous theorems we consider periodic functions. Without loss of generality we adopt  $2\pi$ -periodicity. The following theorem proves the spectral accuracy of a conceptually new finite difference operator. This result is in contrast with the well established property of FDMs having an algebraic rate of convergence. Our nonstandard formulation makes no use of polynomial interpolation, including trigonometric polynomials. The new method arises solely from manipulations of singular integrals as presented in the following theorem.

**Theorem 3.** *Let  $f(x) \in C^m$  be a  $2\pi$ -periodic function. Consider a grid with nodes spaced by  $h = 2\pi/N$ , where  $N$  is a multiple of 4. In approximating the first derivative of  $f(x)$ , there exists a finite difference operator with spectral accuracy, where the error depends on the function's regularity. The multi-level difference operator  $D_{\text{ML}}^1[f]_j$  acts on all grid values  $[f]$  in approximating the derivative  $f'(x_j)$ . The operator is defined through*

$$f'(x_j) \approx D_{\text{ML}}^1[f]_j \equiv -\frac{2}{N^2} \sum_{d \text{ odd}}^{N/2-1} C_d \sum_{\ell \text{ odd}}^{N/2-1} S_\ell^{-2} (D_{j+d,\ell}^2[f] - D_{j-d,\ell}^2[f]). \quad (3)$$

The coefficient  $C_d$  is related to the distance  $dh$  from the target point  $x_j$  to the center of the compact stencil defined by the operators  $D_{j\pm d,\ell}^2$ . The coefficient  $S_\ell$  is related to the resolution level  $\ell$ . These coefficients have the following expressions:

$$C_d = \cot(hd/2) \quad (4)$$

and

$$S_\ell = \frac{\sin(h\ell/2)}{h\ell}. \quad (5)$$

**Proof:** Consider the Hilbert transform on the circle

$$\mathcal{H}[f](x) \equiv \frac{1}{2\pi} \int_0^{2\pi} \cot\left(\frac{x-y}{2}\right) f(y) dy, \quad (6)$$

as well as the Hilbert transform of the derivative of  $f$ , given by

$$\mathcal{H}[f'](x) \equiv \frac{1}{4\pi} \int_0^{2\pi} \frac{f(x) - f(y)}{\sin^2\left(\frac{x-y}{2}\right)} dy. \quad (7)$$

Using the identity  $-\mathcal{H}[\mathcal{H}[f]](x) = f(x)$ , the following expression holds for  $2\pi$ -periodic functions:

$$f'(x) = -\frac{1}{8\pi^2} \int_0^{2\pi} \cot\left(\frac{x-y}{2}\right) \int_0^{2\pi} \left(\frac{f(y) - f(\tilde{y})}{\sin^2\left(\frac{y-\tilde{y}}{2}\right)}\right) d\tilde{y} dy. \quad (8)$$

The ATR, provided by Theorem 2, yields the *spectrally accurate* expression approximating  $f'(x_j)$ :

$$f'_j \approx -\frac{2}{N^2} \sum_{\substack{m=0 \\ (m+j)\text{ odd}}}^{N-1} \cot\left(\frac{h(j-m)}{2}\right) \sum_{\substack{n=0 \\ (m+n)\text{ odd}}}^{N-1} \frac{f_m - f_n}{\sin^2\left(\frac{h(m-n)}{2}\right)}. \quad (9)$$

The above expression can be recast in the form

$$D_{\mathbf{ML}}^1[f]_j \equiv -\frac{2}{N^2} \sum_{d \text{ odd}}^{N/2-1} \cot\left(\frac{h}{2}d\right) \sum_{\ell \text{ odd}}^{N/2-1} \left(\frac{(h\ell)^2}{\sin^2\left(\frac{h}{2}\ell\right)}\right) (D_{j+d,\ell}^2[f] - D_{j-d,\ell}^2[f]), \quad (10)$$

by grouping terms and using the symmetry and the antisymmetry of the respective kernels, when  $d$  or  $\ell$  are greater than  $N/2$ . In this case these indices are relabelled to the equivalent value less than  $N/2$ . Due to the periodic grid-structure, care is needed in the above expression: a renumbering should be performed for the stencil indices  $P = j \pm d \pm \ell$ , when  $P$  falls outside the set  $\{0, 1, 2, \dots, N-1\}$ . The renumbering is straightforward. In the respective difference operator, when  $P < 0$  we redefine  $P := N + P$ . Similarly when  $P > N-1$  we redefine  $P := P - N$ . This is in accordance with the numbering extension indicated by the white squares in the example of figure 2.

The distance coefficient is

$$C_d = \cot\left(\frac{hd}{2}\right), \quad (11)$$

and the resolution-level coefficient are expressed as

$$2S_\ell = \mathcal{S}_L(x)|_{x=h\ell} \equiv \frac{\sin(\pi x/L)}{(\pi x/L)} \Big|_{x=h\ell}; \quad L = 2\pi. \quad (12)$$

This completes the proof.  $\square$

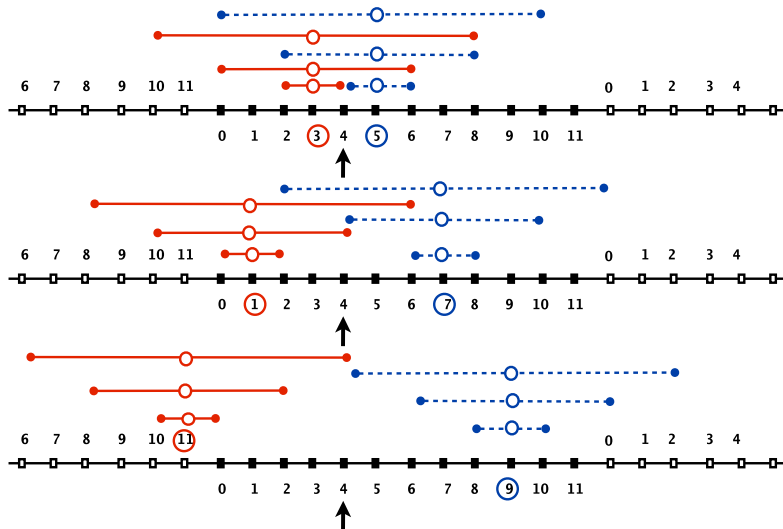


Figure 2: Graphic visualization of the multi-resolution stencils, where  $j = 4$  and  $N = 12$ . Dark squares are the mesh points while white squares are their periodic “extensions”, for a better visualization of the multi-level framework.

New finite differencing properties are readily available through Theorem 3. The present differentiation method approximating  $f'(x)$  is based on numerically integrating diverse estimates of  $f''(x)$ , obtained through compact stencils of various support widths. These *multi-scale* estimates are all of (low)  $2^{nd}$ -order and crude, in the sense that many are evaluated on low-resolution (wide) stencils. Nevertheless it is remarkable that, at the end, the superior spectrally accurate operator is obtained by combining multi-resolution stencils centered at all nodes of the adjoint grid. These combinations are performed through the resolution-level coefficients  $S_\ell$ , which are grid-point values of a (macroscopic) Whittaker cardinal function [10, 9], which equals 1 at the interval’s midpoint and 0 half a period away.

The interpretation from the mathematical, approximation theory, point of view now follows. We interpret  $f(x) \equiv F(x, y = 0)$  as the real-axis trace of a harmonic function  $F$  in the upper half-plane.  $F(x, y)$  is the real part of an upper analytic (complex) function. Expression (9) first performs the discrete Hilbert transform of  $F_x(x, 0)$ . Despite the fact that differentiation commutes with the Hilbert transform, expression (7) is exact and deals directly with increments of  $f$  which is very convenient, since values of  $f'(x)$  are in principle unknown. Due to the Cauchy-Riemann equations, this expression can also be viewed as the Hilbert transform of  $G_y(x, 0)$ , where  $G$  is the

harmonic conjugate of  $F$ . This sets a connection with the interesting work of Squire and Trapp [8], as explained below. They developed a numerical method using complex variables in order to approximate the derivative of real valued functions. Their method gained attention [5] and has been used in many applications, such as numerical Fréchet derivatives [2] as well as in Data Science [1]. As mentioned by Higham [5] “*A fundamental tension in numerical analysis is the interplay between truncation errors and round-off errors; this is particularly prevalent in the numerical approximation of derivatives.*” In order to make finite-difference truncation errors small, one needs to compute with very small values of  $h$ . This choice might influence the buildup of roundoff error and the complex-step method [8] is well suited to avoid this buildup. In our case truncation-errors might already be small due to spectral accuracy. Hence our discretization parameter  $h$  does not need to be very small, as will be numerically illustrated.

The complex-step method of Squire and Trapp [8] extends  $f$  as a complex analytic function, by virtue of  $f(x_j + ih)$ , which by Taylor expansion gives

$$F(z) \equiv f(x_j + ih) = f(x_j) + ihf'(x_j) - 0.5h^2f''(x_j) + \mathcal{O}(h^3).$$

Their second order approximation arises as

$$f'(x_j) \approx \text{Im}(f(x_j + ih))/h. \quad (13)$$

This complex extension of  $f$  automatically implies that the respective harmonic conjugate is zero at  $x_j$ . This fact avoids a subtractive cancellation error [8] present in FDMs when  $h$  is extremely small. The complex-step expression (13) is actually the finite difference approximation of the  $y$ -derivative of the harmonic conjugate, about the real axis. Namely

$$f'(x_j) \approx \frac{\text{Im}(f(x_j + ih)) - \text{Im}(f(x_j))}{h} \quad (14)$$

is a semi-discrete approximation of a Cauchy-Riemann equation along the real axis. In principle this method needs a complex evaluation tool, where care is needed [2]. Our spectrally accurate method presented in Theorem 3 also made use of the  $y$ -derivative of the harmonic conjugate, but without any use of complex functions nor any Taylor expansion. Note that the continuation into the complex plane is different between our method and the complex-step method. Each method generates a different analytic continuation in the upper-half plane where real-axis traces, of the real part, both coincide with  $f(x)$ .

It is instructive to consider a small grid example in order to write explicitly all terms of our numerical scheme. This allows a clear visualization of all stencils activated through the (distribution) kernels. Consider the example

with  $N = 12$  and take as target node  $j = 4$ . Using expression (9) or (10), we have that:

$$f'_4 \approx -\frac{2}{N^2} \cdot \left\{ C_1 \left( \frac{D_{5,1}^2 - D_{3,1}^2}{S_1} + \frac{D_{5,3}^2 - D_{3,3}^2}{S_3} + \frac{D_{5,5}^2 - D_{3,5}^2}{S_5} \right) + \right. \\ \left. + C_3 \left( \frac{D_{7,1}^2 - D_{1,1}^2}{S_1} + \frac{D_{7,3}^2 - D_{1,3}^2}{S_3} + \frac{D_{7,5}^2 - D_{1,5}^2}{S_5} \right) + \right. \\ \left. + C_5 \left( \frac{D_{11,1}^2 - D_{9,1}^2}{S_1} + \frac{D_{11,3}^2 - D_{9,3}^2}{S_3} + \frac{D_{11,5}^2 - D_{9,5}^2}{S_5} \right) \right\}.$$

The stencil notation  $D_{k,\ell}^2$ , as in(10), has the first subscript  $k$  indicating the stencil's center-node, while the second subscript equals half of the stencil's width. The multi-resolution stencils are depicted in figure 2.

These stencils, of varying support width, explore the entire domain always centered on the adjoint grid. This structure is a consequence of convolutions with distributions. We will refer to our method as a distributional finite difference method (dFDM), where stencils of variable compact support test/probe the function's derivative on the entire domain, resulting in approximations of superior accuracy.

## 2.2 The differentiation matrix

The present method and, for example, the Fourier spectral method have the same spectral accuracy. A natural question is whether these methods are identical, where ours operates in the physical domain while the Fast Fourier Transform (FFT) operates in the frequency domain. This is answered by looking at the differentiation matrix of each formulation and by examining, in the next section, the respective roundoff error structure.

The standard centered finite difference is obtained from

$$f'(x_j) = \frac{f(x_{j+1}) - f(x_{j-1}))}{2h} + \frac{h^2}{12} f'''(\xi), \quad x_{j-1} < \xi < x_{j+1}. \quad (15)$$

The differentiation matrix is trivially obtained as

$$\mathcal{D}_{\text{FDM}}^N = \frac{1}{h} \begin{bmatrix} 0 & 1/2 & & \cdots & & -1/2 \\ -1/2 & 0 & 1/2 & & & \\ & -1/2 & 0 & 1/2 & & \\ & & & 0 & & \\ \vdots & & & & \ddots & \vdots \\ \vdots & & & & & 0 & 1/2 \\ 1/2 & \cdots & & & & -1/2 & 0 \end{bmatrix}. \quad (16)$$

The differentiation matrix for the Fourier method is obtained from interpolating  $f(x)$  with a basis of band-limited functions [9]. On the real line  $f(x)$  is approximated by a linear combination of translated Whittaker cardinal functions [10]  $\mathcal{S}_h(x)$ :

$$p(x) = \sum_{m=-\infty}^{\infty} f_m \mathcal{S}_h(x - x_m), \quad (17)$$

where  $\mathcal{S}_h(x) = \sin(\pi x/h)/(\pi x/h)$  are the band-limited functions, whose Fourier spectrum runs exactly up to the Nyquist frequency. The derivative of  $f$  is approximated as

$$f'_j \approx \frac{dp}{dx}(x_j) = \sum_{m=-\infty}^{\infty} f_m \mathcal{S}'_h(x - x_m). \quad (18)$$

In the  $2\pi$ -periodic case a similar interpolation is made, but with periodic sinc functions [9], where

$$p(x) = \sum_{m=1}^N f_m \tilde{\mathcal{S}}_N(x - x_m), \quad \text{with } \tilde{\mathcal{S}}_N(x) \equiv \frac{\sin(\pi x/h)}{(2\pi x/h) \tan(x/2)}, \quad N = 2\pi/h. \quad (19)$$

The functions  $\tilde{\mathcal{S}}_N(x)$  are the periodic counterpart of Whittaker's cardinal functions. The derivative, evaluated at grid-points, equals

$$\tilde{\mathcal{S}}'_N(x_j) = \begin{cases} 0, & j = 0, \\ \frac{1}{2}(-1)^j \cot(jh/2), & j \neq 0. \end{cases} \quad (20)$$

This leads to the differentiation matrix

$$\mathcal{D}_{\text{FFT}}^N = \frac{1}{2} \begin{bmatrix} 0 & \cdots & \cdots & -C_1 \\ -C_1 & 0 & & +C_2 \\ +C_2 & & 0 & -C_3 \\ -C_3 & & & 0 & +C_4 \\ \vdots & & & & \vdots \\ \vdots & & & \ddots & C_1 \\ C_1 & \cdots & \cdots & & 0 \end{bmatrix}, \quad (21)$$

where we recall that  $C_j = \cot(jh/2)$ .

The dFDM differentiation matrix is found by recalling that the ATR uses two grids. To obtain the distributional finite-differencing matrix it is convenient to rewrite expression (9) into two components, one for each grid. Relabelling accordingly yields

$$f'(x_j) \approx -\frac{2}{N^2} \left\{ \alpha_N \sum_{m_1}^{N-1} \left[ \cot\left(\frac{h}{2}(j - m_1)\right) \right] f_{m_1} - \right. \quad (22)$$

$$- \sum_{m_2}^{N-1} \left\{ \sum_{\ell=1, \text{ odd}}^{N/2-1} \frac{\cot(\frac{h}{2}(j-m-\ell)) + \cot(\frac{h}{2}(j-m+\ell))}{\sin^2(\frac{h}{2}\ell)} \right\} f_{m_2}, \quad (23)$$

where

$$\alpha_N \equiv \sum_{\ell=1, \text{ odd}}^{N/2-1} \frac{2}{\sin^2(\frac{h}{2}\ell)}. \quad (24)$$

If the index  $j$  of the target node is even, then indices  $m_1$  are odd-valued while indices  $m_2$  are even. If  $j$  is odd then  $m_1$  runs over the even grid while indices  $m_2$  run over the odd grid. The number 2, which appears in the multi-level coefficient  $\alpha_N$ , is reminiscent of contributions from the center-nodes of the respective stencils. As mentioned earlier, the center of the test-stencils are on the adjoint grid. The diagonal entry, corresponding to  $m_2 = j$ , is zero. The same is true for the entry  $(j, m_2)$ ,  $m_2 = j \pm N/2$ , half a period away.

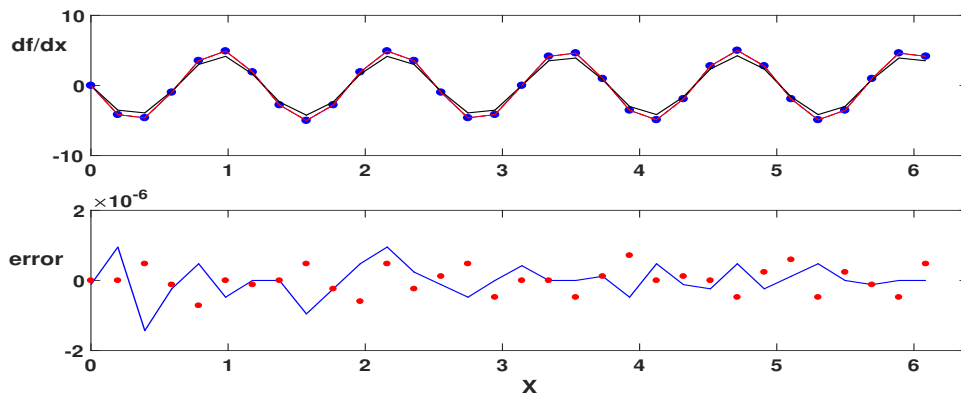


Figure 3: Numerical illustration for  $f(x) = \cos(5x)$ , with  $N = 32$ . Top: Dots display the result from the dFDM. Two lines are superimposed connecting the dots: results from the FFT method and the exact derivative. The solid line with a small discrepancy displays the result from the FDM. Bottom: roundoff error difference (between exact  $f'$  and method) for the dFDM (solid line) and the FFT (dots). The  $\ell_\infty$  norms are:  $\|f'-\text{dFDM}\|_\infty = 1.4 \cdot 10^{-6}$  and  $\|f'-\text{FFT}\|_\infty = 7.1 \cdot 10^{-7}$ .

### 3 Computational illustration

As our first computational illustration we consider  $f(x) = \cos(5x)$  with only  $N = 32$  points. Due to spectral accuracy, the dFDM and the FFT method are exact up to roundoff error. The FDM is of second error. At the top of figure 3 we have the derivative computed by these three methods

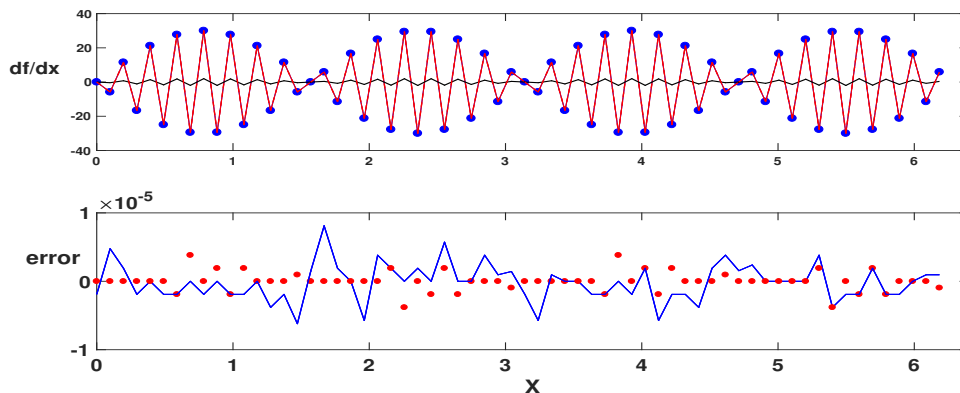


Figure 4: Numerical illustration for  $f(x) = \cos(30x)$ , with  $N = 64$ . The rapidly varying function is almost at the Nyquist frequency. Top: dots display the result from the dFDM. Two lines are superimposed connecting the dots: results from the FFT method and the exact derivative. The solid line with a large discrepancy displays the result from the FDM. This is due to large values of the third derivative in (15). Bottom: the roundoff error difference (between exact  $f'$  and method) for the dFDM (solid line) and the FFT (dots). The  $\ell_\infty$  norms are:  $\|f' - \text{dFDM}\|_\infty = 8.1 \cdot 10^{-6}$  and  $\|f' - \text{FFT}\|_\infty = 3.8 \cdot 10^{-6}$ .

compared to the exact derivative. The dots are values from the dFDM, coinciding with high accuracy with the FFT and the exact solution. In order to better visualize the roundoff error all computations were done in MATLAB using single precision. The roundoff error difference between the FFT and the exact derivative are depicted by dots, in the bottom part of figure 3, while the roundoff error difference between the dFDM and the exact value by a solid line. In the top graph we observe the result with the FDM, in a dark solid line, exhibiting some discrepancy with respect to the other methods.

Next we consider a rapidly varying function:  $f(x) = \cos(30x)$ . We use a grid with  $N = 64$  points. We have a well resolved Fourier mode which is close to the limiting Nyquist frequency. Again the values from our dFDM, the FFT method and the exact derivative coincide with high accuracy. At the top of figure 4 we display these solutions while at the bottom graph the respective roundoff error. At the top graph of figure 4 we see a low amplitude jagged curve representing the FDM approximation which is very poor. This is expected because, as indicated by (15), the FDM's truncation error scales like  $\varepsilon^{-3}$  for rapidly varying functions  $f(x/\varepsilon)$ ,  $\varepsilon \ll 1$ .

In some problems it might be necessary to work with a great number of grid points. In figure 5 we have the derivative of a slowly varying function given by  $f(x) = \cos(x)$ . In this case the truncation error is zero but we test

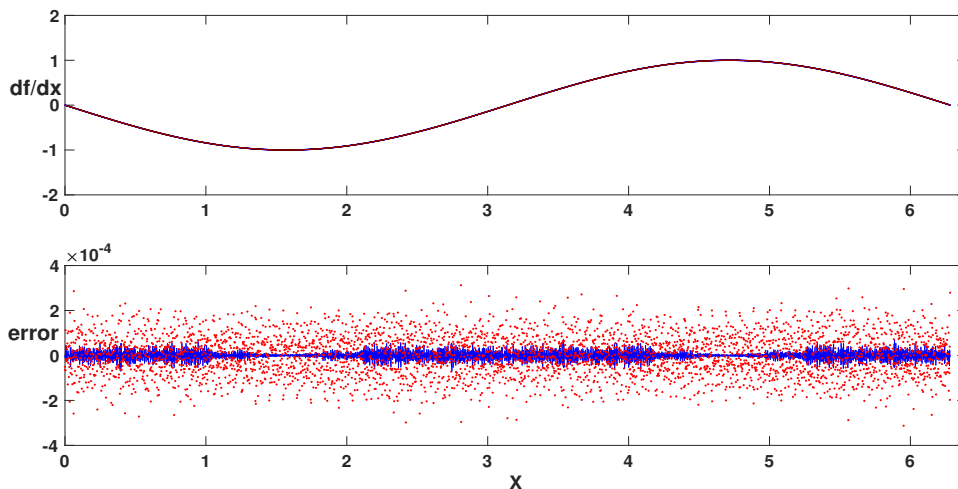


Figure 5: Numerical illustration for  $f(x) = \cos(x)$ , with  $N = 4096$ . Top: Four lines are superimposed: results from the dFDM, the FFT method, the FDM and the exact derivative. We have a slowly varying function and test the methods in the presence of a large number of grid points. The agreement is very good. Bottom: the roundoff error difference (between exact  $f'$  and method) for the dFDM (solid line) and the FFT (dots). The  $\ell_\infty$  norms are:  $\|f' - \text{dFDM}\|_\infty = 7 \cdot 10^{-5}$  and  $\|f' - \text{FFT}\|_\infty = 3.1 \cdot 10^{-4}$ . In figure 6 we take a closer look.

the use of a large number of grid points:  $N = 4096$ . The top graph in figure 5 has three curves, regarding the exact derivative, the result of the dFDM and of the FFT method. The roundoff error difference with the exact solution is displayed at the bottom. The cloud of points regards the FFT method while the solid line regards the dFDM. The roundoff error structure is quite different, where for the dFDM it is non-uniformly distributed. To have a closer look, refer to figure 6 where we have zoomed into the neighborhood of  $x = 3\pi/4$ . We observe that the FFT method displays oscillations due to the amplification of the sawtooth mode, namely at the Nyquist frequency. Differentiation in the FFT method is performed through its Fourier multiplier, where Fourier amplitudes are multiplied by  $ik$ . In the case of a smooth function the upper (inactive) end of the Fourier spectrum is amplified by an order of  $10^3$ . The agreement between the dFDM and the exact derivative is excellent.

Now we consider a function with a full Fourier spectrum. In Fourier space the Gaussian  $f(x) = \exp(-(x - \tilde{x})^2/\delta)$  is also a Gaussian. We choose  $\delta$  so that  $f$  decays fast enough to numerically be well approximated by its periodic extension. At the top of figure 7 we display the function  $f(x)$  while the middle graph superimposes three curves: the exact derivative, and the

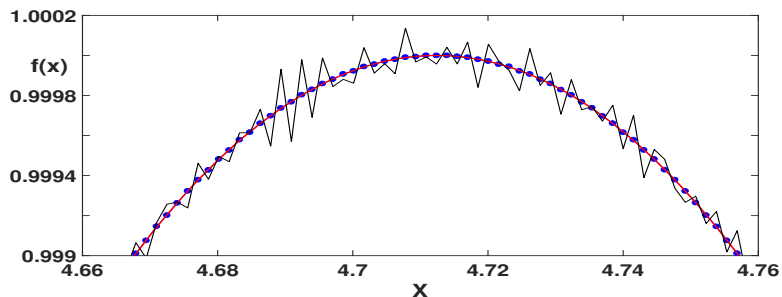


Figure 6: Detail from figure 5. Dots display the result from the dFDM which coincide with the exact derivative. The sawtooth profile regards the FFT method, where Fourier amplitudes are multiplied by  $ik$ . The Nyquist frequency, containing only roundoff error is amplified by  $N/2 = 2048$  and is visible as we zoom into the graph. Nevertheless this is not visible on the original scale depicted in figure 5.

results for the dFDM and the FFT method. A total of  $N = 512$  points were used. The roundoff error is displayed at the bottom part of figure 7. The cloud of points regards the roundoff error difference between the exact derivative and the FFT method. The solid line regards the roundoff error difference from the dFDM. The structure is quite different. While the FFT produces roundoff errors uniformly along grid points, the dFDM produces roundoff error only on points where the function  $f$  is effectively supported. In figure 8 we increase the resolution by using  $N = 2048$  and the structure is unchanged.

The next illustration considers the non-periodic function used by Squire and Trapp [8], in applying their complex-step method. They computed the derivative of  $f(x) = x^{9/2}$  at the point  $\tilde{x} = 1.5$ . Double-precision was considered, so we now adopt double-precision in Matlab. Since our method applies to periodic functions we used a smooth cutoff in the form of a super-Gaussian  $sG(x)$  given by

$$sG(x) = e^{-(\sigma(x-\pi))^s}. \quad (25)$$

To compute the dFDM exactly at  $\tilde{x}$  we perform the shift  $f(x) = (x - \pi + 1.5)^{9/2}$  and therefore centered the super-Gaussian at  $x = \pi$ . Since our method is non-local we explored with different widths of this “table-top” function. We avoid having its effective support in the region where we have the square root of a negative function. We apply the dFDM to the function  $\tilde{f}(x) \equiv f(x) \cdot sG(x)$  in order to compute the derivative at  $x = \pi$ , the shifted position with respect to  $\tilde{x}$  of Squire and Trapp. Excellent results are obtained. In figure 9 we used a super-Gaussian with  $s = 10$ ,  $\sigma = 1.6$  and  $N = 512$ , which yields  $h \approx 0.012$ . The top graph displays the super-Gaussian centered at  $x = \pi$ . The middle graph displays (in dots) the dFDM

solution while in gray we have the exact derivative. The bottom graph depicts the function  $f(x)$ . At the point of interest the exact derivative value, evaluated through Matlab, is  $f' = 18.600812734259758$ . The approximate value computed with the dFDM is  $f'_{257} \approx 18.600812734259215$ . The dFDM value provides 14 digits of accuracy.

Squire and Trapp [8] compare, in Table 1 (page 111), the accuracy of their complex-step method (CSM) with the central finite differencing (FD)  $f' \approx f(1.5 + h) - f(1.5 - h)/(2h)$ . Both methods are second order accurate. We reproduce some entries from their table. For a resolution of  $h = 0.01$ , which corresponds to their first table entry, the FD gives  $f' \approx 18.602018344501897$  while for the CSM they obtain  $f' \approx 18.599607128036329$ . Rounding at the first 4 digits agrees with the exact value. To obtain 14 digits of accuracy the CSM requires  $h = 10^{-7}$  and gives  $f' \approx 18.600812734259637$ . The dFDM obtained 14 digits with  $h = 10^{-2}$ .

We further reduced the resolution to  $N = 128$  ( $h \approx 0.05$ ) using  $s = 8$  and  $\sigma = 3.0$ . These choices provide a sharp super-Gaussian cutoff as shown by the solid line in figure 10. We obtain  $f'_{65} \approx 18.613734049360190$ , namely with 3 digits of accuracy. Due to the low resolution we then explored with a smoother super-Gaussian, adopting  $s = 4$  and  $\sigma = 1.6$ , as depicted by the dotted line in figure 10. We obtain  $f'_{65} \approx 18.600812731981232$ , namely with 10 digits of accuracy. The different super-Gaussians were tested in an experimental fashion. We have not attempted to find it's optimal width.

## 4 Conclusions

The main goal of this work is to present a conceptually new framework for a finite difference operator which, as opposed to other finite differences, has superior spectral accuracy. The method is based solely on numerical manipulations of singular integrals. The singular integral is a convolution with a distribution. The distribution sets the stage for a multi-resolution finite difference operator. The numerical accuracy of the distributional finite difference scheme (dFDM) is illustrated through a series of examples. These are compared with the Fourier (FFT based) spectral method. The FFT method performs differentiation in the frequency domain, whereas the dFDM in the physical domain. It is shown that their roundoff error structure is quite different. The dFDM is also compared with a complex-step method where the goal is to make the truncation error as small as possible by taking a very small step size  $h$ . By construction our truncation error is small for smooth functions, which is a property related to spectral accuracy. We get many digits of accuracy with much larger step sizes.

As themes for future investigation, we consider analyzing other singu-

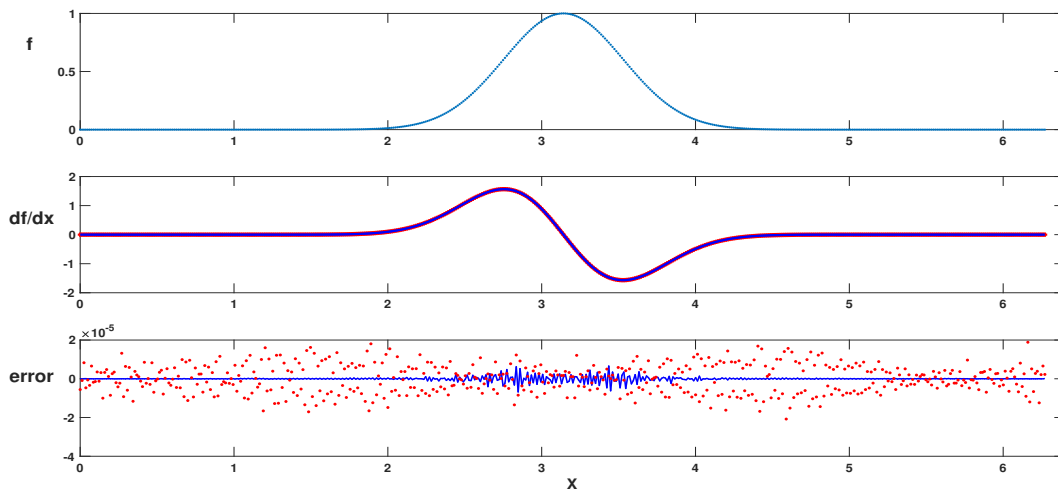


Figure 7: Top: the Gaussian  $f(x) = \exp(-(x - \pi)^2/0.3)$ . The grid has  $N = 512$  points. Middle: three curves coincide, namely the exact derivative, the dFDM and the FFT method. Bottom: the roundoff error difference for the dFDM (solid line) and the FFT method (dots). The  $\ell_\infty$  norms are:  $\|f'-\text{dFDM}\|_\infty = 7.8 \cdot 10^{-6}$  and  $\|f'-\text{FFT}\|_\infty = 2.1 \cdot 10^{-5}$ .

lar integral strategies, the possibility of the making the scheme more compact and efficient computationally while exploring applications to differential equations.

The author's work was supported in part by CNPq under (PQ-1B) 301949/2007-7 and FAPERJ Cientistas do Nosso Estado project no. 102.917/2011.

## References

- [1] I. GOODFELLOW, Y. BENGIO and A. COURVILLE, *Deep Learning*, Cambridge, MA, MIT Press, 2016.
- [2] A. AL-MOHY and N.J. HIGHAM, The complex step approximation to the Fréchet derivative of a matrix function. *Numer. Algor.*, 53:133-148 (2010).
- [3] C. CANUTO, M.Y. HUSSAINI, A. QUARTERONI and T.A. ZANG *Spectral Methods in Fluid Dynamics*, Springer Verlag, 1988.
- [4] B. FORNBERG, On a Fourier method for the integration of hyperbolic equations, *SIAM J. Num. Anal.*, vol. 12, pp. 509–528 (1975).
- [5] N.J. HIGHAM, Differentiation With(out) a Difference. *SIAM News*, June, (2018).

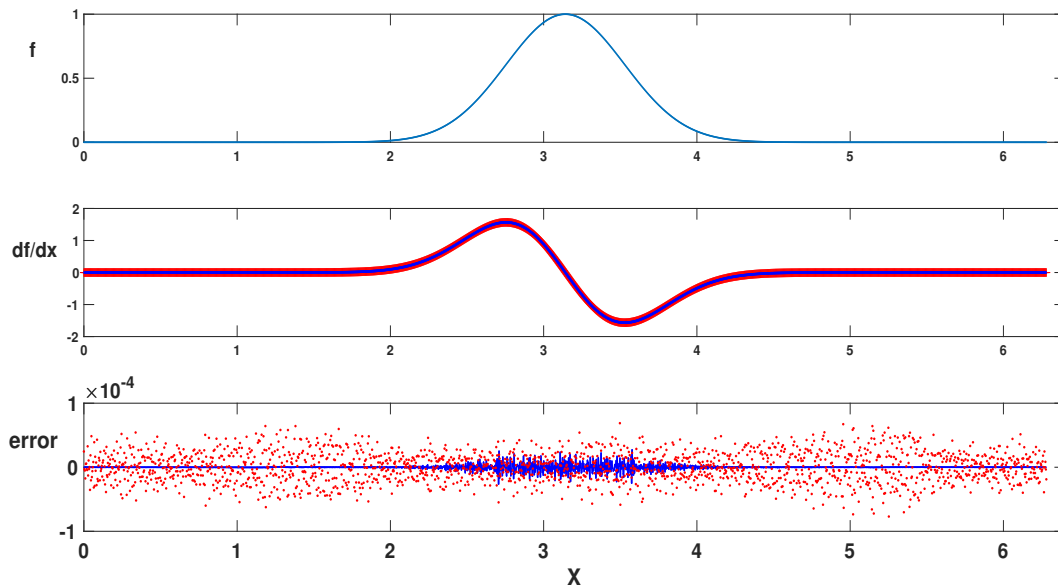


Figure 8: Top: the Gaussian  $f(x) = \exp(-(x - \pi)^2/0.3)$ . The grid has  $N = 2048$  points. Middle: three curves coincide, namely the exact derivative, the dFDM and the FFT method. Bottom: the roundoff error difference for the dFDM (solid line) and the FFT method (dots). The  $\ell_\infty$  norms are:  $\|f' - \text{dFDM}\|_\infty = 2.7 \cdot 10^{-5}$  and  $\|f' - \text{FFT}\|_\infty = 7.7 \cdot 10^{-5}$ .

- [6] R.D. RICHTMYER and K.W. MORTON. *Difference Methods of Initial-Value Problems*, Krieger Publishing Company, 2nd. Ed., 1967.
- [7] A. SIDI and M. ISRAELI, Quadrature methods for periodic singular and weakly singular Fredholm integral equations. *J. Sci. Comput.*, Vol. 3, 2:201-231 (1988).
- [8] W. SQUIRE and G. TRAPP, Using complex variables to estimate derivatives of real functions, *SIAM Rev.*, Vol. 40, 1:110-112 (1998).
- [9] L.N. TREFETHEN. *Spectral Method in MATLAB*, Cambridge University Press, 2000.
- [10] E.T. WHITTAKER, On the functions which are represented by the expansions of the interpolation theory, *Proc. Roy. Soc. Edinburgh*, 35:181–194 (1915).

IMPA, INSTITUTO NACIONAL DE MATEMÁTICA PURA E APLICADA, RIO DE JANEIRO, BRASIL.  
*E-mail: nachbin@impa.br*

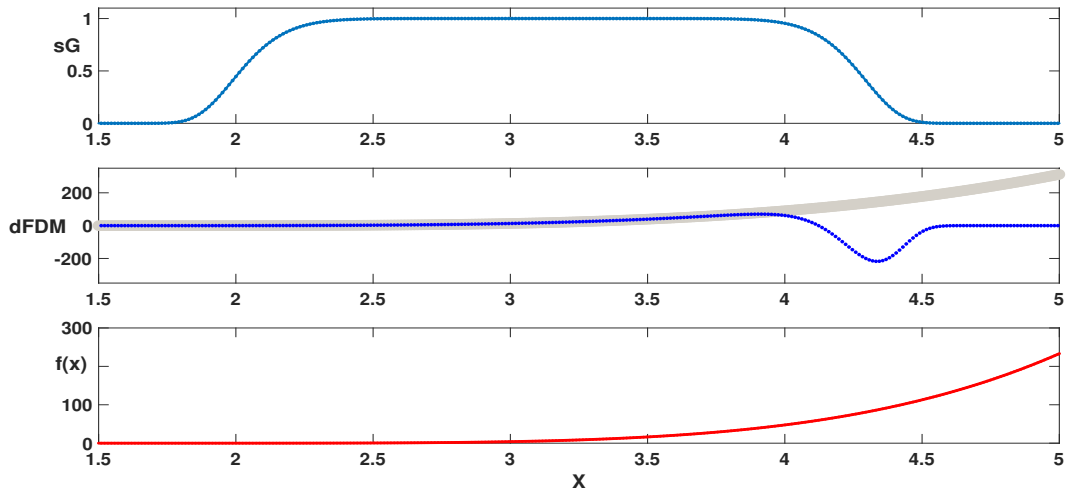


Figure 9: Top: the super-Gaussian  $sG(x)$  centered at  $x = \pi$ , our point of interest, with  $s = 10$  and  $\sigma = 1.6$ . We have zoomed into the region of interest. Middle: the dFDM derivative appears in dots ( $N = 512$ ). The exact derivative is displayed in gray. The agreement at  $x = \pi$  is up to 14 digits of accuracy. Bottom: the function  $f(x)$ .

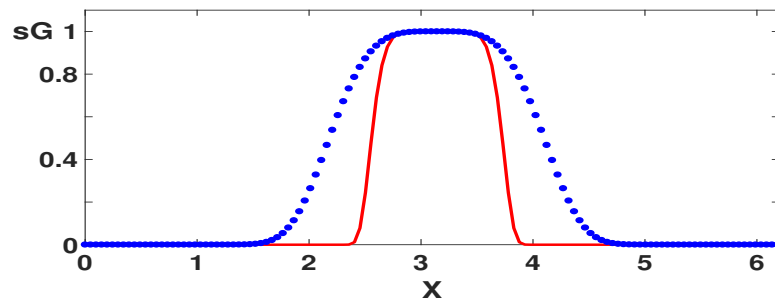


Figure 10: A low resolution example with  $N = 128$ . Two super-Gaussians  $sG(x)$  were tested, both centered at  $\pi$ . The  $sG$  depicted with dots used  $s = 4$  and  $\sigma = 1.6$  while the  $sG$  with a solid line  $s = 8$  and  $\sigma = 3.0$ .